Synthesis, morphological structures and material characterization of electrospun PLA : PCL/magnetic nanoparticle composites for drug delivery

Hazim J. Haroosh[1], Yu Dong[2,*], Gordon D. Ingram[1]

[1]*Department of Chemical Engineering, Curtin University, Perth, WA 6845, Australia*

[2]*Department of Mechanical Engineering, Curtin University, Perth, WA 6845, Australia*

ABSTRACT

The effects of pure and impure magnetic nanoparticles (MPs) with three different concentrations (0.01, 0.1 and 1 wt%/v) on the morphological structure, crystallinity level, thermal properties and constituent interactions of electrospun poly(lactic acid) (PLA): poly(ε-caprolactone) (PCL) based composites were investigated by means of scanning electron microscopy (SEM), transmission electron microscopy (TEM), X-ray diffraction (XRD), differential scanning calorimetry (DSC), gel permeation chromatography (GPC), Fourier transform infrared spectroscopy (FTIR) and drug release tests using UV–vis spectrophotometry. Tetracycline hydrochloride (TCH), as a typical therapeutic compound, was loaded into these composite fibrous structures to study their application for drug delivery. The infrared spectra of composite nanofibers confirm the successful embedding of MPs into the fibrous networks. The addition of pure MPs increased the solution viscosity and thus promoted the MP dispersion inside the electrospun composite fiber mats. Impure MPs led to considerably lower average fiber diameters, and could generate unique cell structures that were reported for the first time in this study. The accelerated release of TCH was found by adding pure MPs to PLA: PCL blends. This

*Corresponding author. Tel.: +61 8 92669055; fax: +61 8 92662681.
E-mail address: Y.Dong@curtin.edu.au(Y. Dong).

characteristic was reflected in the parameters of Ritger-Peppas and Zeng models, which were well fitted to our experimental drug release data.

Keywords: Nanoparticles; Electrospinning; Drug delivery system; Non-woven fabrics

INTRODUCTION

Nanotechnology is dealing with synthetic and natural formations of materials and devices at a nanoscale level, specifically in the range of 1 nm to 1 µm.[1] Diverse approaches have been undertaken in recent years to produce nanostructures or nanomaterials, such as phase separation, self-assembly and electrospinning. Among these methods, electrospinning is a very simple and versatile polymer processing technique for synthesizing nanofibers in non-woven fabric structures. In electrospinning, a flow of a polymer melt or solution often leads to a few jets being driven out to form the "Taylor cone" in a high-voltage electric field.[2] These jets are pulled out from the droplet surface and drawn into fibrous structures in the direction of the collecting plate. Electrospinning is a promising process for many biomedical applications, especially in controlled drug delivery systems that have been investigated in recent decades.[3] Besides, this kind of system has some significant medical benefits like nontoxic degradation in the human body and sustained release of encapsulated drugs.[4]

PLA is a semi-crystalline polymer that is broadly used in a range of biomedical applications due to its dissolvability in common solvents, biodegradability, good mechanical properties and biocompatibility.[5,6] PCL is another semi-crystalline polymer widely used in tissue scaffolding due to its good drug permeability and slow biodegradability.[7] Furthermore, PCL is frequently applied in long-term implantable foundations. Magnetic nanoparticles such as Fe_3O_4 are inorganic materials having low toxicity, super-paramagnetic properties, good biocompatibility, easy preparation[8] and better stability in the atmosphere than metal nanoparticles.[9]

Recently, a variety of sophisticated techniques have been developed to prepare hybrid nanofiber system for different biomedical applications.[10-13] In previous work, we also found novel electrospun nanocomposite fibers by embedding halloysite nanotubes (HNTs) with biocompatible polymeric solution to overcome the weak interaction between hydrophilic drug and hydrophobic polymer.[14,15] Loading drugs into electrospun nanofibers has attracted great attention because this system possesses good structural stability and higher efficiency of drug encapsulation than any other drug delivery medium.[16] One complex factor is that loading a drug into the polymer solution influences the solution properties, such as its viscosity.[17] In addition, the drug release from a fiber mat can be controlled by the alterations of the fiber morphology, polymer composition and drug loading method.[18] Tetracycline hydrochloride (TCH) is an antibiotic often used for the healing and prevention of bacterial infections in burns, cuts, other injuries and surgery, as well as in many other wound healing areas.

The purpose of this work is to ultimately produce a novel electrospun hybrid composite material by mixing PLA: PCL blends with MPs, which may be potentially used to create a new drug delivery system that enables directed drug release to a targeted body area by using external magnetic fields. The main focus of this paper is the holistic evaluation of electrospun PLA: PCL/MP composites in a systematic manner, from their fabrication, structural analysis and material characterization to drug release tests, which are then interpreted by typical mathematical models for drug release kinetics.

MATERIALS AND METHODS

Materials

PLA 3051D pellets with molecular weight (MW) = 93,500 g/mol and glass transition temperature T_g = 65.50°C,[19] were supplied by NatureWorks, USA. Other materials, used

as-received in this study, including PCL with *MW*= 80,000 g/mol, iron sulfate, iron nitrate, sodium hydroxide, lauric acid, tetracycline hydrochloride (TCH, $C_{22}H_{24}N_2O_8 \cdot HCl$ and *MW*=480.9 g/mol), phosphate buffer solution (PBS), chloroform and methanol, were purchased from Sigma-Aldrich Ltd, Australia. Iron sulfate and iron nitrate were selected to synthesize MPs. PBS acted as a medium of drug release while TCH worked as a model antibacterial drug with its excellent ultraviolet (UV) chromophore. Chloroform and methanol were employed as solvents for the PLA: PCL blends.

Synthesis of magnetic nanoparticles (MPs)

Iron sulfate ($FeSO_4$) and iron nitrate ($Fe(NO_3)_3$) were dissolved in deionized water to prepare an aqueous solution with a 2:1 molar ratio of Fe(III) to Fe(II). After vigorous stirring at 80°C for 1 h, a 1-molar solution of NaOH was added dropwise to achieve a prepared solution with pH =12; a black precipitate then formed as an indicator of magnetite's presence. Impure MPs were obtained by drying the black precipitate without any purification. In order to prepare pure MPs, 1 ml lauric acid was added to the solution to coat the MPs. Then the black precipitate was centrifuged and washed several times with deionized water before final drying to produce black powders. The chemical reaction for the MP synthesis is expressed in equation (1). Both pure and impure MPs were considered in this study because we expected to assess the effect of the salts present in the impure MPs on the fibre diameter and morphology. It is well known that salts in polymeric solution enhance its electrical conductivity, which is one of significant factors in the electrospinning process.

$$FeSO_4(s)+2Fe(NO_3)_3(s)+8NaOH\ (aq) \longrightarrow Fe_3O_4(s)+Na_2SO_4(aq)+6NaNO_3(aq) + 4H_2O\ (l) \quad (1)$$

Electrospinning

Electrospinning was carried out using a mix of 8 wt%/v PLA and 15 wt%/v PCL solutions at a volume ratio of 1:1. The solvent used in all cases was a mix of chloroform

and methanol (2:1 volume ratio). The pure and impure MPs at three different concentrations of 0.01, 0.1 and 1 wt%/v were added to the PLA: PCL blend solution, and subsequently mixed by using an ultrasonicator for 2 h. For the drug loading, 5 wt% TCH was mixed with 0.1 and 1 wt%/v MPs for 2 h in methanol using a similar ultrasonication method, and then they were added to the blended solution. In the electrospinning process, the different types of solutions were transferred to a 10ml syringe pump (A Fusion 100 syringe pump, Chemyx Inc. Stafford, TX USA) with a needle specification of 20G (approximately 0.584 mm inner diameter). The solution flow rate was set at 2 ml/h, and the applied positive voltage was in the range of 25–28 kV. The electrospinning process was conducted at 24ºC, and the resulting fibers were collected on flat aluminium foils covering a ground collector with the needle-to-collector distance at 13 cm. The thickness of fiber mats was in range of 330 to 450 µm directly measured by a micrometer.

In vitro drug release study

The drug-loaded fiber mat sample (2 cm×2 cm) was incubated in 20 ml PBS (pH=7.4) using a rotary shaker at 37°C. After the required incubation time for drug release, the sample was transferred to 20 ml fresh buffer solution and 36 separate incubations were completed to obtain the TCH release data points for three nanofiber mats. After that step, the amount of TCH released in the buffer solution was determined accordingly.

Characterization techniques

Solution viscosity was measured by using a Visco 88 portable viscometer from Malvern Instruments (UK), which has a built-in temperature sensor and is supplied with a double gap measuring geometry to provide extra sensitivity when measuring low-viscosity fluids. The shear rate was changed from 0 – 20000 s^{-1} depending on the solution viscosity of the polymer, where all the samples were measured at room temperature of 23°C. The electrical conductivity and pH value of the solution were measured by using a WP-81

Waterproof pH and Conductivity Meter (TPS, Australia). The morphology of electrospun nanofibers was studied via an EVO 40XVP scanning electron microscope (SEM) (Germany) at an accelerating voltage of 5 kV. Before SEM observation, the samples were sputter-coated with platinum. Average fiber diameter was calculated from the SEM images by using an image analysis tool in the Zeiss Smart SEM software. For each sample, measurements were made for a minimum of 150 fibers from multiple scanned SEM images and at a rate of approximately 15 fibers per image.

The electrospun nanofibers were embedded in Araldite® epoxy resin by using the following method to control the fiber homogeneity and distribution: About $1cm^3$ of epoxy was polymerized in advance without embedding the fiber mat. The fiber mat was then macerated in the epoxy, placed on the solidified epoxy that had been pre-polymerized, and subsequently the composites were re-polymerized. The epoxy block, containing the present embedded fiber mat, was sectioned into 100 nm layers using a diamond knife with a Leica EM UC6 microtome, and the sections were later mounted onto carbon grids. Observations for MP dispersion level were performed using a JEOL 2011 transmission electron microscope at an accelerating voltage of 200 kV

XRD measurements of prepared mat samples were performed in a Bruker Discover 8 X-ray diffractometer (Germany) operated at 40 kV and 40 mA. A Cu-Kα radiation source was used to scan samples in a 2θ range from 5° to 40° with a scanning rate of 0.05°/s. This source was monochromatized with graphite sample monochromators. The *d*-spacing (*d*) was determined from Bragg's law ($n\lambda=2d\sin\theta$) where θ is the diffraction angle, λ is the wavelength (λ= 1.54 Å for a Cu target), and *n* is an integer.

The crystallite size (*L*) was calculated from the Scherrer relation[20] ($L=K\lambda/B\cos\theta$). Here *B* is the complete width at half maxima of the crystalline peak in radians, and *K* is the shape factor of the average crystallite. The level of crystallinity was determined by

implementing the area integration method from XRD intensity data over the range of 2θ from 8° to 27°.[20]

Thermal analysis was performed using a DSC6000 Perkin Elmer (USA) with Cryofill liquid nitrogen cooling system. Approximately 10 mg of cut fiber mat was sealed in an aluminium pan. The thermal behavior was analyzed during the first heating scan between –90°C to 200°C with a ramp rate of 10°C/min.

Fourier transform infrared spectroscopy (FTIR) was carried out in a Spectrum 100 FTIR Spectrometer Perkin Elmer (Japan). Spectra were recorded in a range of 4000–550 cm^{-1} with 4 cm^{-1} resolution by using an attenuated total reflectance (ATR) technique.[21] FTIR was used to investigate the interaction level between MPs and PLA: PCL blends.

Gel permeation chromatography (GPC) analysis was undertaken to find the molecular weight of polymer blends using one ShodexKF-805L and three KF803L columns connected in series operated at 40°C, with a UV detector and Shodex DS-4 pump. Tetrahydrofuran (THF) was used as the eluent at a flow rate of 1.0 ml/min.

The amount of TCH detected in the release buffer was determined by a UV–vis spectrophotometer (JascoV-67) at a wavelength of 360 nm.

RESULTS AND DISCUSSION

Pure MPs and TCH

To investigate the effect of MPs, PLA: PCL blend solution was mixed with pure MPs at 0.01, 0.1 and 1 wt%/v. Figure 1 reveals that with the addition of MPs, solution viscosities and electrical conductivities tended to be enhanced with increasing the MP concentration. As seen from Figure 2, the addition of pure MPs in the composite system appears to produce more uniform fibrous structures with smaller fiber diameters as opposed to electrospun PLA: PCL fibers. The corresponding calculated average fiber diameters are reported in Table 1. It is evident that average fiber diameter was reduced greatly from

711 to 583 nm when the MP concentration increased from 0.01 to 1 wt%/v, which is well below that of PLA: PCL fiber at 814 nm.

On the other hand, Figure 2(e)–(g) and Table 1 demonstrate that the addition of 5 wt% TCH into PLA: PCL based composites with 0, 0.1 and 1 wt%/v MPs facilitates the reduction of average fiber diameter from 623 to 491 nm. All these materials become smaller than their counterparts without TCH. Two primary parameters of electrospinning process, solution viscosity and electrical conductivity, both increase remarkably when the MP concentration increases from 0 to 1 wt%/v, Figure 1. The additional amphoteric molecules of TCH, having several ionizable functional groups,[22] further increase the solution conductivity as compared to those without TCH. This implies that electrical conductivity plays a relatively dominant role in determining fiber morphology despite the addition of MPs increasing the solution viscosity.

It was previously reported that decreasing the solution viscosity resulted in a decrease of the fiber diameter,[23] whilst a higher electrical conductivity produced electrospun fibers with smaller diameters. The decreased nanofiber diameters found in this study could be ascribed to the predominant effect of the significant increase of electrical conductivity relative to a modest increase of solution viscosity. In terms of the effect of electrical conductivity, as shown in Figure 1, an increase in the MP concentration leads to the enhancement in the electrical conductivity, apparently due to the increase of the iron content. More importantly, the presence of TCH can significantly enhance the electrical conductivity of electrospun composite fibers, especially at the MP concentrations of 0–0.1wt%/v. As a matter of fact, the increased electrical conductivity inevitably produces more electric charges that are carried by the electrospinning jet. Consequently, higher repulsive forces are imposed on the jet in order to elongate the jet materials into fibrous structures in the electrical field.[24] Furthermore, by increasing the electrical conductivity,

the draw rate and large draw ratio of the jet in its bending instability area can be increased during electrospinning. Hence, the induced jet path becomes longer and experiences a more stretching process from the solution droplets. Both higher repulsive forces and greater bending instability could contribute to electrospun fibers with smaller diameters.[25,26]

Impure MPs

PLA: PCL blend solution was mixed with 0.01, 0.1 and 1 wt%/v impure MPs to produce electrospun composite fibers. As illustrated in Figure 3 and Table 1, relatively tiny fiber diameters, about one-tenth of those of PLA: PCL blend fibers with pure MPs, were observed. The average fiber diameter decreases from 80 to 51 nm when the impure MP concentration increases from 0.01 to 1 wt%/v. This phenomenon could be explained by the dual effect of a sharp decline in solution viscosity and significant enhancement of electrical conductivity with increasing the impure MP concentration from 0 to 1 wt%/v. Both solution viscosity and electrical conductivity of composites with impure MPs are much more sensitive to MP concentration than their counterparts with pure MPs, Figures. 1 and 4. The solution viscosity abruptly drops from 476 to 13 cP with impure MPs compared to a very modest increase from 476 to 522 cP with pure MPs. As mentioned earlier, a simultaneously significant decrease in the solution viscosity and increase in the electrical conductivity inevitably result in the reduction of fiber diameters.

More interestingly, the fibrous structures also contain nearly 3D spherical cells with rough nuclei diameters ranging from 1 to 10 μm. The fibers radiate away from a central nucleus and these cells became larger and more aggregated with increasing the MP concentration, especially as shown in Figures 3(b) and (c). Each cell is isolated from other cells by borders, which is formed by bundles of overlapping fibers. The fibers line up around the nuclei, and more aligned fibers are visible in the central area of nuclei, as

evidenced in Figures 5(a) and (b). The fibers were found to disappear from the nuclei when the MP concentration increases, which might be due to the sharp decline in the solution viscosity, leading to the frequent formation of small fiber diameters and beads. These unique material structures and behavior are reported for the first time through this study, and have not been mentioned elsewhere in the previous literature. The nuclei look like aggregated MPs as a result of the low solution viscosity. Accordingly, small MPs tend to easily move through the solution due to their magnetization, huge surface area and high surface energy, which allow them to aggregate and attract one another. The reorientation of MP positions may lead to the alignment of MPs with the applied electrical field after the solvent removal in the electrospinning process.

The sharp drop in the solution viscosity is due to the impurities present in the untreated magnetic nanoparticles, consisting of the salts like sodium sulfate, sodium nitrate and sodium hydroxide. It was found in this study that the impurities lead to the reduced molecular weight of PLA: PCL blends, from 84700 g/mol in the neat polymer blend down to 62700, 20200 and 12600 g/mol at three impure MP concentrations of 0.01, 0.1 and 1wt%/v, respectively, Figure 6. In comparison, as a typical attempt, only the molecular weight of 1wt%/v pure MPs (due to its highest particle concentration) was measured, which was found to be 81000 g/mol (not shown in Figure 6), relatively comparable to that of PLA: PLC blends. As a result, there may be less significant effect on the molecular weight at even lower concentrations of pure MPs than 1 wt%/v. The remarkable decline in molecular weight of impure MPs may also account for the sodium sulphate to react with PLA: PCL blends, resulting in the cleavage of PLA: PCL molecular chains into smaller fragments. In addition, when sodium nitrate loses an oxygen atom, it causes the formation of sodium nitrite, which decreases the polymerization rate and in turn contributes to a decrease of the molecular weight for

polymer blends.[27] Furthermore, the OH group reacts with the ester bonds to generate intermediate degradation polymers, after which further cleavage of the initial products into fractions with lower molecular weights occurs.[28] It was found that the pure MPs did not affect the pH value of PLA: PCL blend solution; whereas impure MPs conversely increase the pH value of the solution. By adding 0.01, 0.1 and 1 wt%/v MPs, the pH values have been increased to 12.11, 12.32 and 12.76, respectively, as compared with a pH value of 6.88 for the PLA: PCL blend. This phenomenon could be due to the hydrogen bonding being disturbed through the depolymerisation process, which can increase pH value, decrease molecular weight and improve the polymer solubility in good accordance with the previous similar finding for chitosan polymer.[29]

The degree of impure MP dispersion inside the electrospun PLA: PCL composite nuclei within the epoxy matrices was investigated by TEM, where the elemental compositions of the impure MPs were confirmed by energy disperse spectroscopy (EDS). Figure 7 shows a TEM image and EDS spectra of morphological structures for 0.1 wt%/v impure MPs. Evidently, a major portion of impure MPs aggregate inside large nuclei, which is in good agreement with the previous SEM results. The average diameters of impure MPs are about 15–35 nm according to the imaging analysis based on counting 200 particles from eight TEM images. As shown in the EDS spectra of the nuclei, the peaks of Fe and O elements suggest that the hybrid nanocomposites contain Fe_3O_4. The presence of Na shows the existence of impure MPs in the mixture, resulting in the reduced molecular weight of PLA: PCL blends. The peak of the C element is associated with PLA: PCL nanofibers accordingly.

Crystallinity and thermal properties

The identified crystalline structures of MPs are illustrated in Figure 8(a), with XRD patterns obtained from pure and impure MPs. The peaks were labelled with the XRD

reflection, and the crystal planes (*hkl*) corresponding to the main crystalline peaks were directly detected in the DICVOL program of the FullProf software.[30] Pure MPs possess the same pattern as that of crystalline magnetite, which includes six diffraction peaks (220), (311), (400), (422), (511) and (440) detected at 2θ = 30.1, 34.3, 43.1, 53.4, 57.2 and 63.2°, respectively. Their corresponding *d*-spacing values are determined as 0.29, 0.25, 0.21, 0.17, 0.16 and 0.14 nm accordingly, in good accordance with those of typical magnetite (Fe_3O_4). As for impure MPs, there were other diffraction peaks (112) and (202) detected at 2θ = 39.2 and 41.5°, signifying the existence of sodium carbonate (Na_2CO_3) due to the impurity effect. This component may have been produced when impure MPs were synthesized. Sodium hydroxide (NaOH) is in contact with atmospheric air and adsorbs CO_2 to form Na_2CO_3 when added dropwise to the MP solution, as expressed in equation (2):

$$2NaOH(aq) + CO_2(g) \longrightarrow Na_2CO_3(aq) + H_2O(l) \quad (2)$$

In addition, it appears that the high peak labelled (220) and (002) at 2θ = 30.1º actually consists of two overlapping peaks for impure MPs. The average crystal size (*L*) of MPs based on the Scherrer relation is on the order of 20±5 and 40±5 nm for pure and impure MPs, respectively.

Figure 8(b) also shows the XRD patterns for PLA: PCL/MP composite fibers with 1 wt%/v impure MPs, and 0.1 and 1 wt%/v pure MPs. Most XRD patterns possess two diffraction peaks (101) and (200) without any significant difference in the peak position, which indicates that the addition of MPs and TCH has very minor effect on the alteration of crystalline structures in the composite fibers.

The XRD data were used to determine the degree of crystallinity in Figure 9. It has been observed that without TCH, the degree of crystallinity of PLA: PCL/MP composites decreases significantly when increasing pure MP concentration. Such a decreasing

tendency might be explained by the abundant nucleation cores that produce a proliferation of tiny crystallites leading to a low degree of overall crystallinity.[31] Furthermore, the presence of 5 wt%/v TCH also causes a moderate decrease of degree of crystallinity as compared to PLA: PCL blends. The crystallinity is reduced more remarkably when pure MPs are concurrently added at levels from 0 to 1 wt%/v. Both MPs and TCH appear to greatly accelerate the nucleation process. Consequently, this phenomenon results in a shorter period for the disentanglement of molecular chains. The associated degree of crystallinity is generally influenced by the restricted mobility of polymer chains, which prevents the good growth of developed crystals.

Conversely, the addition of impure MPs gives rise to an increase in the degree of crystallinity owing to the impurities that can reduce the molecular weight of PLA: PCL blends. Due to the low molecular weight, the short polymer chains could be mostly crystallized through the electrospinning process, as opposed to the large entangled chains of the high molecular weight blends, leading to more amorphous phases. Besides, the regular rearrangement through the solidification process can be hindered by the longer polymer chains, resulting in the lower mobility and greater intermolecular entanglement.[32]

The DSC thermal properties of electrospun composite fibers are shown along with those of neat PCL and PLA: PCL blends in Figure 10 and Table 2. The glass transition temperature (T_g) of PCL within fiber composites decreases remarkably. Moreover, there was a slight decline in melting temperature (T_m) values of both PLA and PCL when increasing the MP concentration from 0 to 1 wt%/v with the addition of 5 wt% TCH. The decrease of T_g is attributed to the dual effect of incorporation of magnetite particles with an anisotropic character, in good accordance with previous work,[33] as well as blending of TCH with its low molecular weight. The TCH molecules with short chains result in a

decreased packing density of polymer chains, and thus facilitate the chain mobility leading to the lower T_g. Additionally, the electrospinning process and resulting fiber diameters can also influence the directional mobility of polymer chains to induce a difference in T_g.[34] The embedded MPs in PLA: PCL blends have been found to slightly decrease the crystallisation temperature (T_c) of PLA. The role of MPs in promoting the heterogeneous nucleation of polymer molecules are not strongly shown, which might be attributed to the low MP concentration. The T_g of PLA within the blends is difficult to observe because it overlaps with the melting peak of PCL. On the contrary, the presence of TCH within the composite fibers leads to the significant increase of T_c, being over 102ºC as opposed to 84ºC for PLA in PLA: PCL blends. This phenomenon implies that the low molecular weight TCH can preclude the cold crystallisation process of PLA, acting as an anti-nucleating agent that, however, might be in an opposite role of MPs.

The incorporation of impure MPs to PLA: PCL blends leads to the noticeable increase in the T_c of PLA. However, there was no significant change to T_g and T_m values of PCL, which is attributed to the significant decrease in the molecular weight of polymer blends. This influence of impure MPs on the molecular weight was much greater for PLA as opposed to PCL. The main reason is that the amount of PCL almost doubles that of PLA in their blend. It also lies in the relatively low crystallinity of PLA, which undergoes a more rapid process of ester hydrolysis compared with PCL. This can cause an increased concentration of ester groups easily attainable in the PLA.[35] Consequently, the impurities associated with MPs are able to react faster with PLA, which might make it more difficult to detect the T_m for PLA.

FTIR evaluation

Fourier transform infrared spectroscopy (FTIR) was used to show possible interactions between MPs and biopolymers. As demonstrated in Figure11(a), the IR spectra of MPs

exhibit the bands in the low frequency region between 1050 and 550 cm^{-1} due to the absorption band of Fe–O. For pure MPs, the band existing at 1636 cm^{-1} is associated with the water deformation, whilst the peak at 3200 cm^{-1} is related to the O–H group, which is due to the hydroxyl group of lauric acid. For impure MPs, new bands exist at 1424 and 1156 cm^{-1}, which are assigned to inorganic nitrates and sulphates, respectively. In addition, there are some shifts in Fe–O bands probably due to differences in the particle sizes of pure and impure MPs. The surface bond force constant increases when the size of MPs becomes very small, resulting in the reorganization of electrons on the particle surface owing to the destruction of many bonds between the surface atoms.[36]

Figure 11(b) shows the FTIR spectra of PLA: PCL and MPs inside the PLA: PCL based composites. PLA: PCL nanofibers at 1757cm^{-1} for PLA and 1724 cm^{-1} for PCL exhibit initially two carbonyl stretching (C=O) bands. Comparison of the spectra of PLA: PCL, PLA: PCL/pure MP composites and PLA: PCL/impure MP composites demonstrates a range of phenomena including peak shifting, appearance or complete disappearance. The single PLA: PCL band at 1184 cm^{-1} is broadened and shifted to lower wave numbers of 1179 and 1175 cm^{-1} when incorporating pure and impure MPs into PLA: PCL blends, respectively. In addition, the presence of the Fe–O band at 583 cm^{-1} confirms the successful embedding of characteristic bands of PLA: PCL and MPs in the infrared spectra of the final composite fibers. Furthermore, the peaks of PLA within PLA: PCL blends occur at both 1757 cm^{-1} and 1088 cm^{-1}, which reflect carbonyl stretching C=O band and C–O stretching band, respectively. These peaks disappeared when the impure MPs were embedded. It can be proven that there is a significant interaction between PLA: PCL blends and impure MPs due to the impurities associated with the MPs as described previously. Such a result supports the findings from the DSC data that suggest a greater impact of impure MPs on PLA compared to PCL.

The spectrum of TCH within PLA: PCL blends was difficult to be assigned for the band shifting. However, the bands of TCH at 1614 and1581 cm^{-1} were observed in PLA: PCL blends, which are allocated to the C=O stretching at ring A and the C=O stretching at ring C, respectively.

In vitro drug release study

Composite fiber mats containing only pure MPs were selected to study drug release. Impure MPs lead to non-uniform fibrous structures with cell aggregation and small fiber diameters (Figures. 3 and 5), making them unsuitable for the drug release application. TCH release profiles from electrospun composite fiber mats with and without pure MPs are presented in Figure 12. Composite fiber mats are shown to offer a sustained drug release performance, though a certain degree of fast drug release appears within the first 5 h (62% for PLA: PCL/1wt%/v MPs, 46% for PLA: PCL/0.1wt%/v MPs, and 42% for PLA: PCL samples). This is followed by a gradual steady release over the total evaluation period of 10 days. The fast release is related to the electrospinning process, which includes the fast evaporation of the solvent and high ionic interactions, leading to the drug being located on the surfaces of electrospun fibers. It was found that TCH was released more rapidly when MPs were added to polymer blends. The difference in cumulative release (%), when adding 1 wt%/v MPs, becomes fairly great compared to those composites without MPs. As for 0.1 wt%/v MPs, such great difference only becomes quite significant after 50 h. TCH release was due to many factors such as drug diffusion through the pores, biodegradation of electrospun fibers and the interaction between TCH and the PLA: PCL/MP composite fiber mats. Due to their nanoscale size, the incorporation of MPs leads to increased fiber porosity,[37] and the porosity can further increase by increasing MP concentration from 0.1 to 1 wt%/v to promote the acceleration of TCH release. In addition, the small diameters of PLA: PCL/MP composite fibrous

structures, compared with their PLA: PCL blend counterparts, certainly increases the surface area, which presents a short diffusion distance with a fast TCH release. Moreover, the low crystallinity of PLA: PCL/MP composite fibers can also assist in the enhancement of fast fiber degradability for the long-term TCH release.

Drug release kinetics

The release kinetics were examined by fitting the drug release data to five mathematical models, namely the zero order, first order, Higuchi[38], Ritger-Peppas[38] and Zeng[39] models. The equations of individual mathematical models and their reported best-fit parameters are listed in Table 3. The R^2 value is the highest when fitting the experimental data to Ritger-Peppas and Zeng models. According to the *n* value of Ritger-Peppas model, the drug release mechanism follows the Fickian transport phenomenon[38] ($n \leq 0.5$) with dominant diffusion process. In addition, increasing MP concentration demonstrates a decrease in *n* values. This mechanism may indicate that the reduction of nanofiber diameters and increase in pore size in the presence of MPs increase the influx of the PBS into the TCH loaded into the nanofiber mat. According to Zeng model, the diffusion process and interaction between PLA: PCL and TCH appear to make a significant impact on the drug release. ΔG refers to the quantities of free and bound drug within electrospun nanofibers. The addition of 0.1 wt%/v MPs to PLA: PCL blends results in the decreasing of ΔG value from -2.0×10^{-22} to -2.6×10^{-22}J, which means that there is a remarkable improvement in the interaction between the drug carrier and TCH. Nevertheless, such improvement cannot adjust the TCH release, and the burst release may be higher than the release from PLA: PCL/TCH. This observation could be due to the small fiber diameters generated by adding MPs, which gives rise to the acceleration of TCH release. In addition, the fast release is due to the increase in the fiber pore size, which is described by increased values of K_s with the addition of MPs. On the other hand, the incorporation

of 1wt%/v MPs suggests a weaker interaction between the carrier and TCH while the number and size of fiber pores appear to grow more. The TCH release might not fit completely with these models because they have a limited applicability, which signifies that they do not consider the erosion, biodegradation or dimensional alteration of the drug carrier.

CONCLUSIONS

This investigation focused on the structure and morphological properties of electrospun nanofibers embedded with three different concentrations of MPs. Both pure MPs and impure MPs were studied to examine TCH release kinetics and interpret the release data with some typical mathematical models. Increasing the pure MP concentrations was found to decrease the average fiber diameter, and this decreasing trend is more significant for impure MPs. However, the addition of the drug TCH to electrospun composite fibers results in smaller fiber diameters. This effect is attributed to two important factors, namely electrical conductivity and viscosity of prepared solutions. Pure MP dispersion is better in the polymer blend structure compared with impure MPs. Impure MPs produce non-uniform fibrous structures and small fiber diameters, making them unsuitable for the drug release application. However, the formation of these novel cell structures has not been mentioned elsewhere in the previous literature. The use of pure MPs and impure MPs leads to very different thermal properties. The degree of crystallinity and the T_g of PCL decrease when pure MPs is mixed with PLA: PCL blends. Conversely, incorporating impure MPs increases the degree of crystallinity with little sign of the melting temperature of PLA. The infrared spectra of electrospun composite nanofibers have proven the successful embedding of MPs into the nanofibers. Impure MPs appear to significantly affect the connecting bonds of PLA. The use of TCH leads to a decrease in T_g and T_m values of PCL and also produces a slight change in T_m values of PLA. The

addition of MPs to PLA: PCL blends is also shown to accelerate the TCH release process. The experimentally determined data for the release kinetics were well fitted with Ritger-Peppas and Zeng models.

ACKNOWLEDGEMENTS

The financial support of Curtin Internal Research Grants (IRG) 2010 (Project No.: 47604) to Dr. Yu Dong is gratefully acknowledged. The authors also wish to thank Ms. Elaine Miller and Dr. Cat Kealley from the Department of Medical Imaging and Applied Physics, Curtin University as well as Prof. Shin-ichi Yusa from University of Hyogo for technical assistance with SEM, XRD and GPC, respectively.

REFERENCES AND NOTES

1 R. Qi, R. Guo, M. Shen, X. Cao, L. Zhang, J. Xu, J. Yu, X. Shi, *J. Mater. Chem.* **2010**, *20*, 10622-10629.

2 Y. Ji, K. Ghosh, B. Li, J. C. Sokolov, R. A. F. Clark, M.H. Rafailovich, *Macromol. Biosci.* **2006**, *6*, 811-817.

3 E. R. Kenawy, F. I. Abdel-Hay, M. H. El-Newehy, G. E. Wnek, *Mater. Chem. Phys.* **2009**, *113*, 296-302.

4 D. Yang, Y. Li, J. Nie, *Carbohydr. Polym.* **2007**, *69*, 538-543.

5 W. Cui, X. Li, X. Zhu, G. Yu, S. Zhou, J. Weng, *Biomacromolecules* **2006**, *7*, 1623-1629.

6 K. Kim, M. Yu, X. Zong, J.Chiu, D. Fang, Y.S. Seo, B.S. Hsiao, B. Chu, M. Hadjiargyrou, *Biomaterials* **2003**, *24*, 4977-4985.

7 J. Han, C. Branford-White, L. Zhu, *Carbohydr. Polym.* **2010**, *79*, 214-218.

8 G. Lv, F. He, X. Wang, F. Gao, G. Zhang, T. Wang, H. Jiang, C. Wu, D. Guo, X. Li, B. Chen, Z.Gu, *Langmuir* **2008**, *24*, 2151-2156.

9 D. Zhang, A.B. Karki, D. Rutman, D.P. Young, A. Wang, D. Cocke, T. H. Ho, Z. Guo, *Polymer* **2009**, *50*, 4189-4198.

10 R. Qi, R. Guo, F. Zheng, H. Liu, J. Yu and X. Shi, *Colloid Surf. B-Biointerfaces* **2013**,110, 148-155.

11 F. Zheng, S. Wang, S. Wen, M. Shen, M. Zhu and X. Shi, *Biomaterials*, **2013**, 34, 1402-1412.

12 S. Wang, F. Zheng, Y. Huang, Y. Fang, M. Shen, M. Zhu and X. Shi, *ACS appl. Mater. & Interfaces* **2012**, 4, 6393-6401.

13 F. Zheng, S. Wang, M. Shen, M. Zhu and X. Shi, *Polym. Chem*. **2013**, 4, 933-941.

14 H. J. Haroosh, D. S. Chaudhary and Y. Dong, *Appl. Polym. Sci*. **2012**, 124, 3930-3939.

15 H. J. Haroosh, Y. Dong, D. S. Chaudhary, G. D. Ingram and S. Yusa, *Appl.Phys. A-Mater. Sci. & Process.* **2013,** 110, 433-442.

16 X. Xu, W. Zhong, S. Zhou, A. Trajtman, M.Alfa, *Appl. Polym. Sci*. **2010**, *118*,588-595.

17 G. Buschle-Diller, J. Cooper, Z. Xie, Y. Wu, J. Waldrup, X. Ren, *Cellulose* **2007**, *14*, 553-562.

18 G. Kim, H. Yoon, Y. Park, *Appl. Phys. A-Mater. Sci. Process.* **2010**, *100*, 1197-1204.

19 P. Haque, I. A. Barker, A. Parsons, K. J. Thurecht, I. Ahmed, G.S. Walker, C.D. Rudd, D. J. Irvine, *J. Polym. Sci. Part A: Polym. Chem*. **2010**, *48*, 3082-3094.

20 N. Ning, Q.Yin, F. Luo, Q. Zhang, R. Du, Q. Fu, *Polymer* **2007**, *48*, 7374-7384.

21 K. K. Chittur, *Biomaterials* **1998**, *19*, 357-369.

22 S.A. Sassman, L.S.Lee, *Environ. Sci. Technol.***2005**, *39*, 7452-7459.

23 Y. Ji, K. Ghosh, X.Z. Shu, B. Li, J.C. Sokolov, G.D. Prestwich, R.A. Clark, M.H. Rafailovich, *Biomaterials* **2006**, *27*, 3782-3792.

24 M. Zamani, M. Morshed, J. Varshosaz, M. Jannesari, *Eur. J. Pharm. Biopharm.* **2010**, *75*, 179-185.

25 G. Lee, J. Song, K. Yoon, *Macromol. Res.* **2010**, *18*, 571-576.

26 A. Saraf, G. Lozier, A. Haesslein, F.K. Kasper, R.M. Raphael, L. S. Baggett, A.G. Mikos, *Tissue Eng. Part C: Methods* **2009**, *15*, 333-344.

27 C. Detrembleur, P. Teyssie, R. Jérôme, *Macromolecules* **2002**, *35*, 1611-1621.

28 K. Makino, H. Ohshima, T. Hondo, *J. Microencapsul.* **1986**, *3*, 203-212.

29 S. Mao, X. Shuai, F. Unger, M. Siomon, D. Bi, T. Kissel, *Int. J. Pharm.* **2004**, *281*, 45-54.

30 A. Boultif, D. Louer, *J. Appl. Crystallogr.* **2004**, *37*, 724-731.

31 J. H. Lee, T. G. Park, H. S. Park, D. S. Lee, Y.K. Lee, S.C. Yoon, J. D. Nam, *Biomaterials* **2003**, *24*, 2773-2778.

32 T. Suwa, M. Takehisa, S. Machi, *J. Appl. Polym. Sci.* **1973**, *17*, 3253-3257.

33 R.V. Kumar, Y. Koltypin, Y.S. Cohen, Y. Cohen, D. Aurbach, O. Palchik, I. Felner, A. Gedanken, *J. Mater. Chem.* **2000**, *10*, 1125-1129.

34 P. H. S. Picciani, E. S. Medeiros, Z. Pan, D. F. Wood, W. J. Orts, L. H. C. Mattoso, B. G. Soares, *Macromol. Mater. Eng*. **2010**, *295*, 618-627.

35 C. G. Pitt, M. M. Gratzl, G.L. Kimmel, J. Surles, A. Schindler, *Biomaterials* **1981**, *2*, 215-220.

36 A. Khan, *Mater. Lett.* **2008**, *62*, 898-902.

37 T. Mikołajczyk, M. Olejnik, *J. Appl. Polym. Sci.* **2006**, *100*, 3323-3331.

38 X. Cai, Y. Luan, Q. Dong, W. Shao, Z. Li, Z. Zhao, *Int. J. Pharm.* **2011**, *419*, 240–246.

39 L. Zeng, L. An, X. Wu, *J. Drug Deliv*. **2011**, *Article ID 370308*, 15 pages.

LIST OF FIGURES

FIGURE 1 Effect of pure MP concentration on the viscosity of PLA: PCL blend solution (1:1 volume ratio) and on the electrical conductivity of PLA: PCL blend solution with 5 wt% TCH.

FIGURE 2 SEM micrographs of electrospun PLA: PCL/ pure MPs composites: (a) 0 wt%/v MPs, (b) 0.01 wt%/v MPs, (c) 0.1 wt%/v MPs, (d) 1 wt%/v MPs, (e) 0 wt%/v MPs and 5 wt% TCH, (f) 0.1 wt%/v MPs and 5 wt% TCH, and (g) 1 wt%/v MPs and 5 wt% TCH. The scale bars represent 10 μm.

FIGURE 3 SEM micrographs of electrospun PLA: PCL/impure MP composites: (a) 0.01wt%/v impure MPs, (b) 0.1wt%/v impure MPs, and (c) 1wt%/v impure MPs. The scale bars represent 10 μm.

FIGURE 4 Effect of impure MP concentration on (a) solution viscosity and (b) electrical conductivity of the PLA: PCL blend solution.

FIGURE 5 SEM micrographs showing electrospun composite fibers lining up around the nuclei: (a) 0.01wt%/v impure MPs and (b) 0.1wt%/v impure MPs. The scale bars represent 2 μm.

FIGURE 6 Effect of impure MP concentration on the molecular weight of the PLA: PCL blends.

FIGURE 7 Typical TEM image and EDS spectra of epoxy/electrospun PLA: PCL composite fibers embedded with impure MPs.

FIGURE 8 XRD patterns for selected materials showing the relative positions of the diffraction peaks (a) impure and pure MPs, and (b) PLA: PCL/MP composites.

FIGURE 9 The degree of crystallinity X_c for PLA: PCL blends and PLA: PCL based composite fibers with pure and impure MPs, as well as TCH. The X_c values were calculated from XRD data.

FIGURE 10 DSC thermograms for selected material samples.

FIGURE 11 FTIR spectra for selected material samples showing the relative FTIR peaks: (a) pure and impure MPs and (b) PLA: PCL based composites with pure and impure MPs and TCH.

FIGURE 12 TCH release profiles from PLA: PCL and PLA: PCL/pure MP composites.

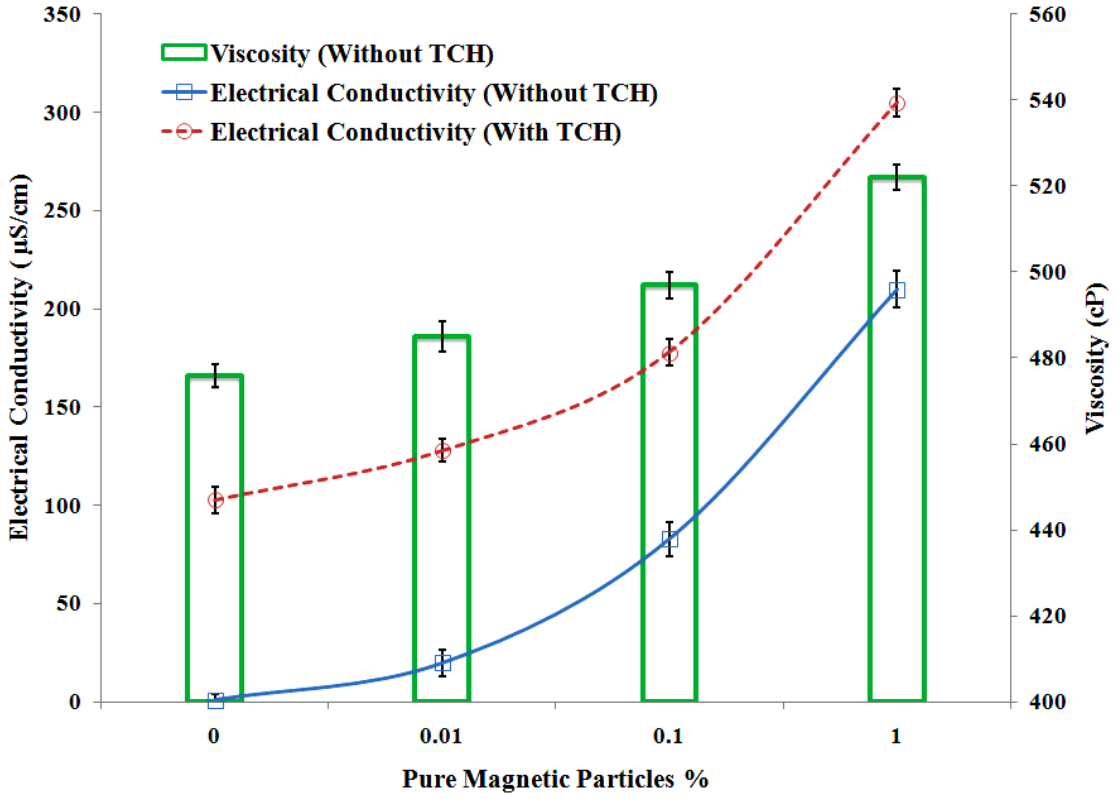
Viscosity (Without TCH)
Electrical Conductivity (Without TCH)
Electrical Conductivity (With TCH)
Electrical Conductivity (µS/cm)
Viscosity (cP)
Pure Magnetic Particles %
0
0.01
0.1
1
350
300
250
200
150
100
50
0
560
540
520
500
480
460
440
420
400

FIGURE 1

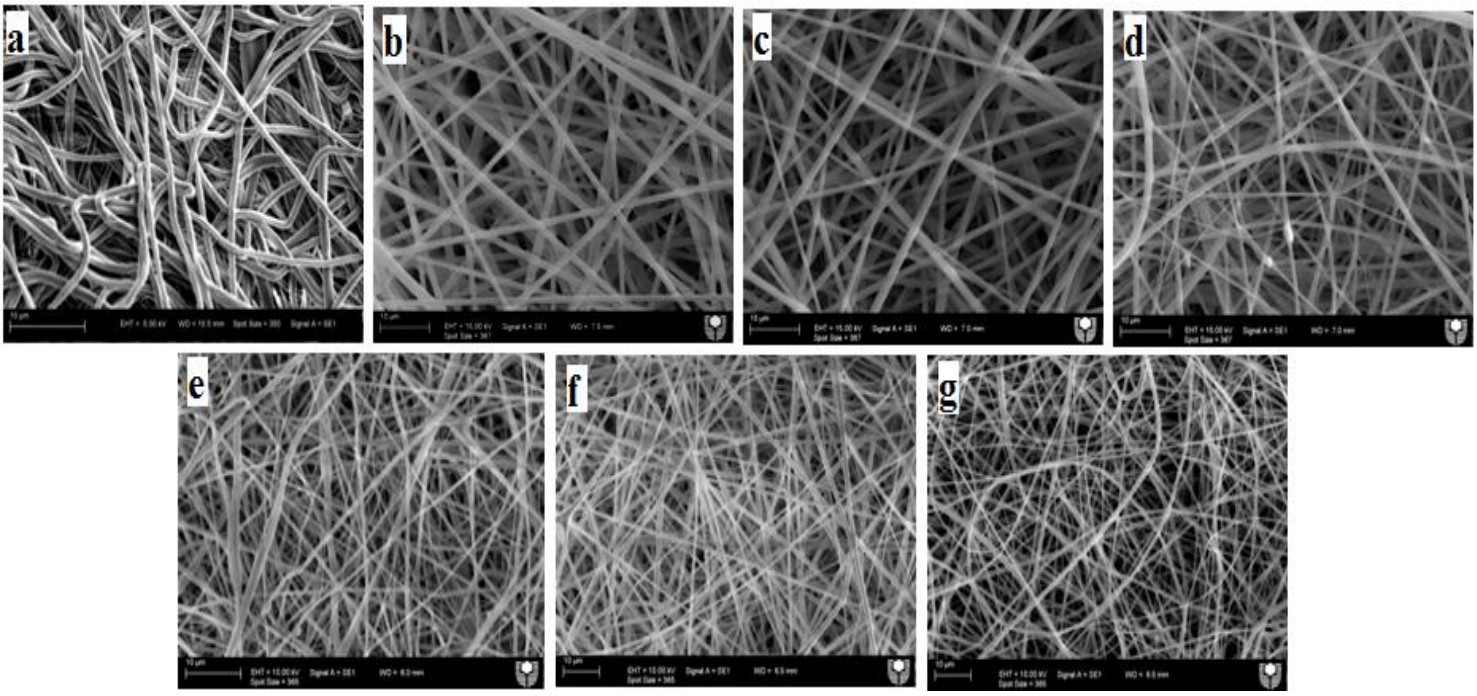

FIGURE 2

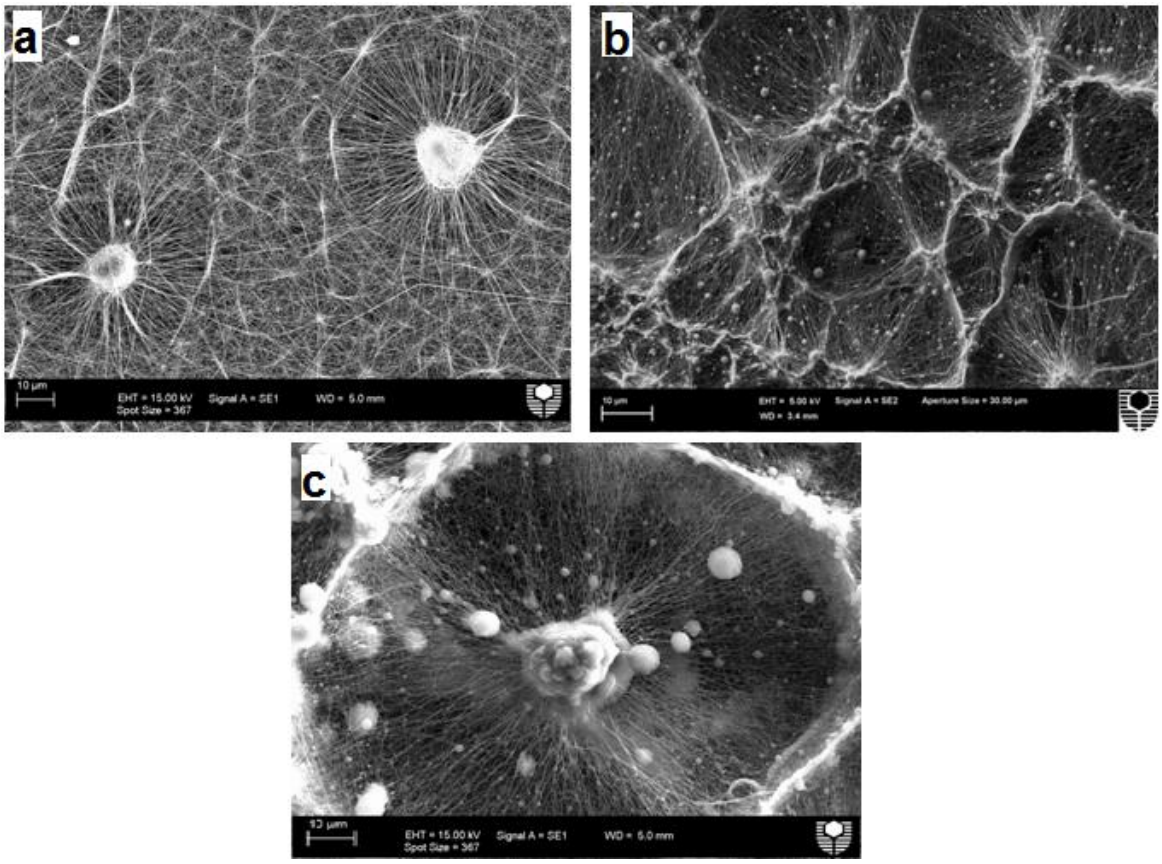
a
10 µm
EHT = 15.00 kV
Spot Size = 367
Signal A = SE1
WD = 5.0 mm
b
10 µm
EHT = 5.00 kV
WD = 3.4 mm
Signal A = SE2
Aperture Size = 30.00 µm
c
10 µm
EHT = 15.00 kV
Spot Size = 367
Signal A = SE1
WD = 5.0 mm

FIGURE 3

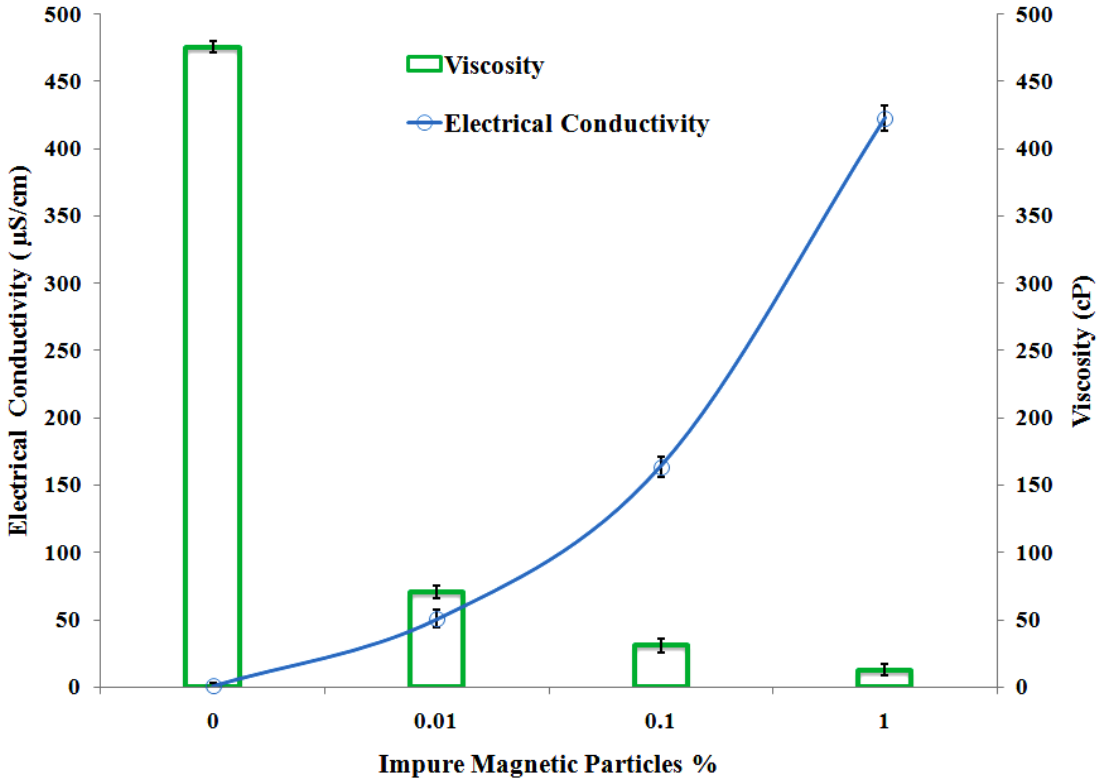
Viscosity
Electrical Conductivity
Electrical Conductivity (µS/cm)
Viscosity (cP)
500
450
400
350
300
250
200
150
100
50
0
0
0.01
0.1
1
Impure Magnetic Particles %

FIGURE 4

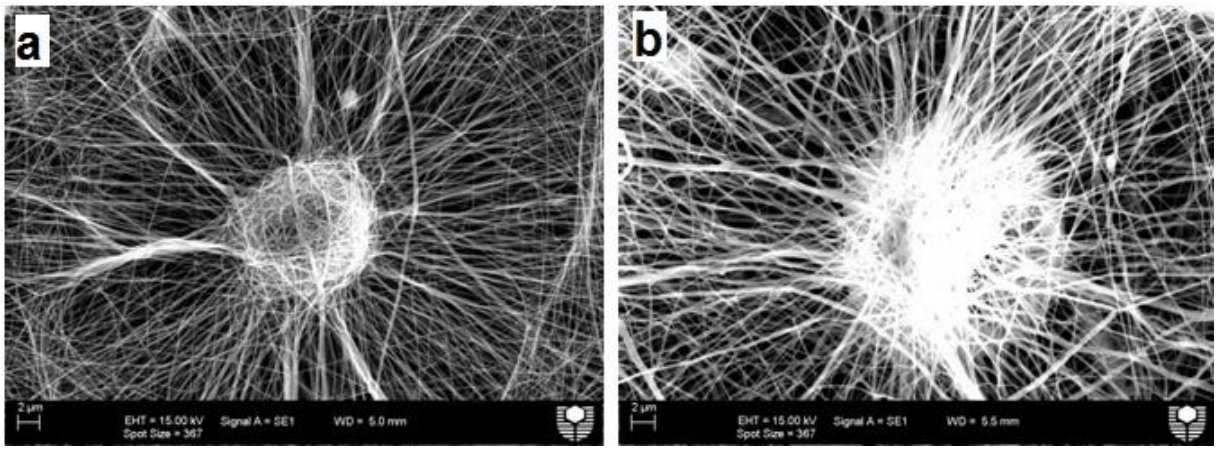
a
2 µm
EHT = 15.00 kV
Spot Size = 367
Signal A = SE1
WD = 5.0 mm
b
2 µm
EHT = 15.00 kV
Spot Size = 367
Signal A = SE1
WD = 5.5 mm

FIGURE 5

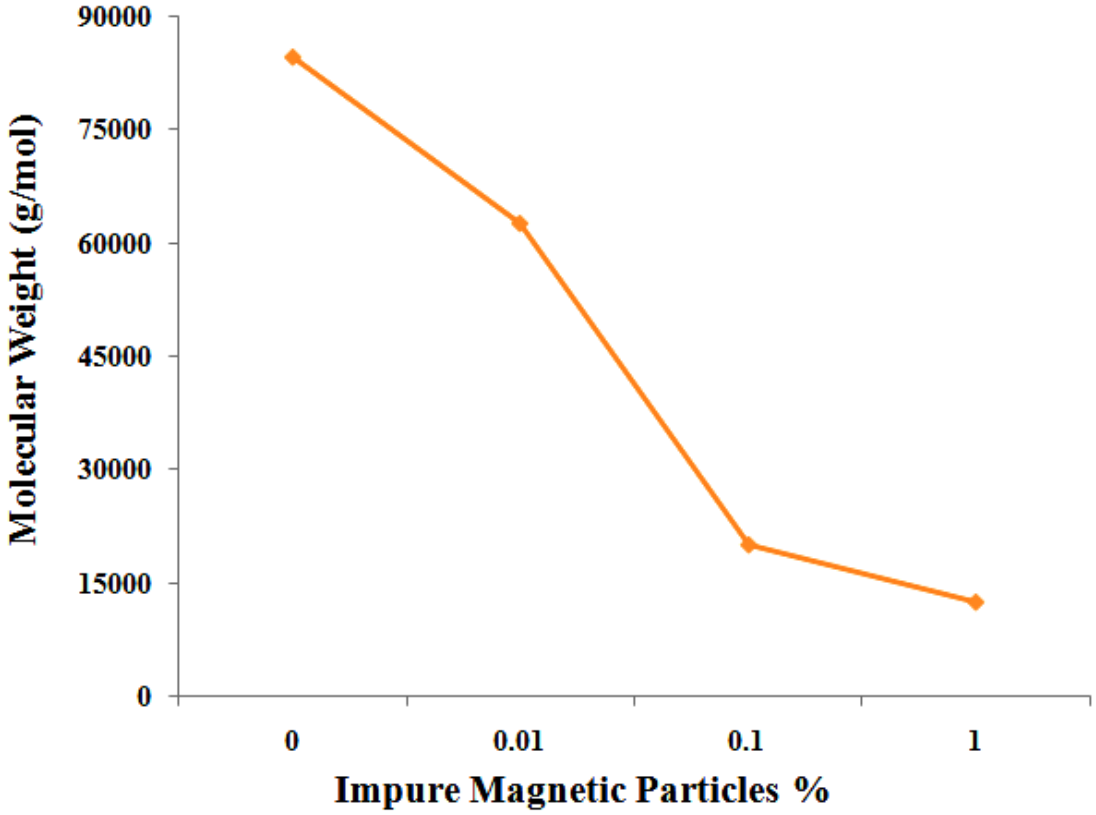
90000
75000
60000
45000
30000
15000
0
Molecular Weight (g/mol)
0
0.01
0.1
1
Impure Magnetic Particles %

FIGURE 6

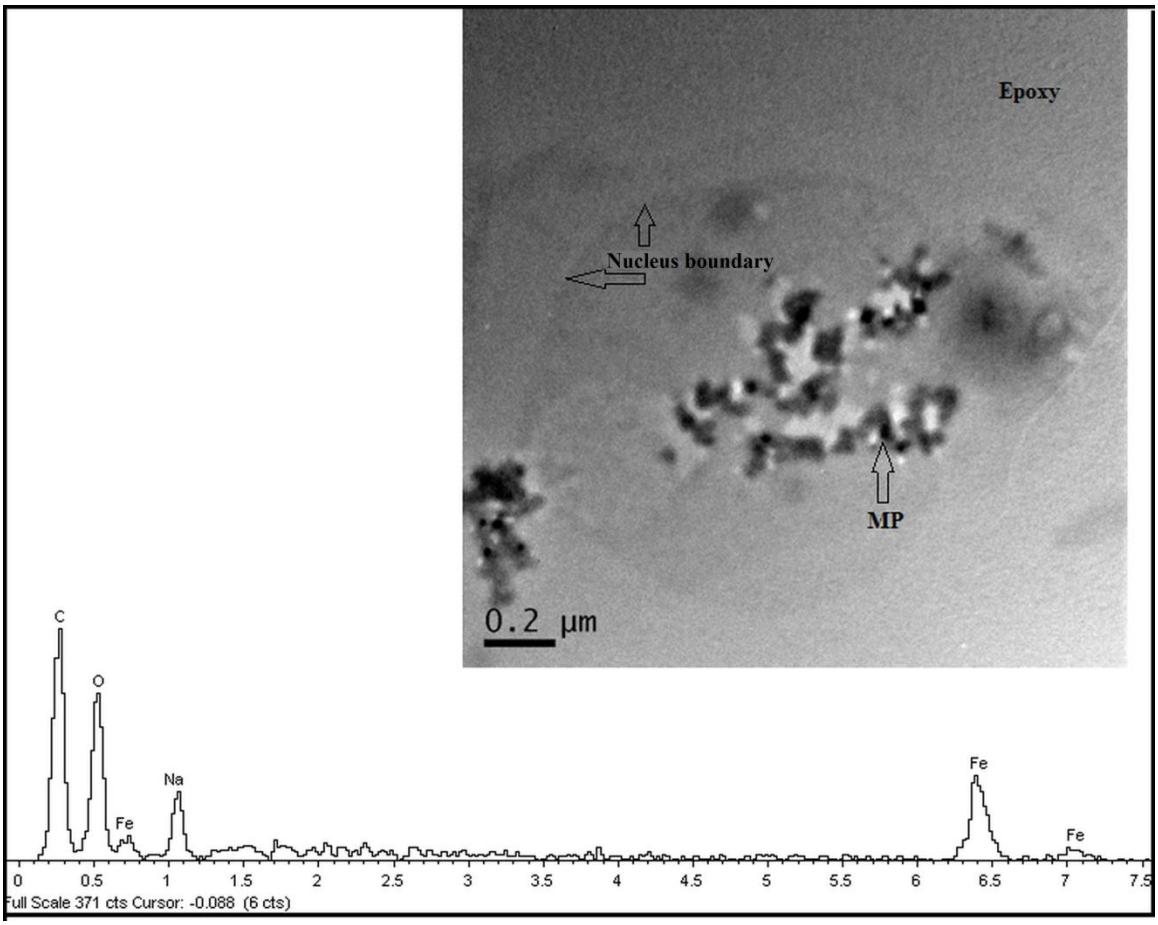
Epoxy
Nucleus boundary
MP
0.2 µm
C
O
Na
Fe
Fe
Fe
0
0.5
1
1.5
2
2.5
3
3.5
4
4.5
5
5.5
6
6.5
7
7.5
Full Scale 371 cts Cursor: -0.088 (6 cts)

FIGURE 7

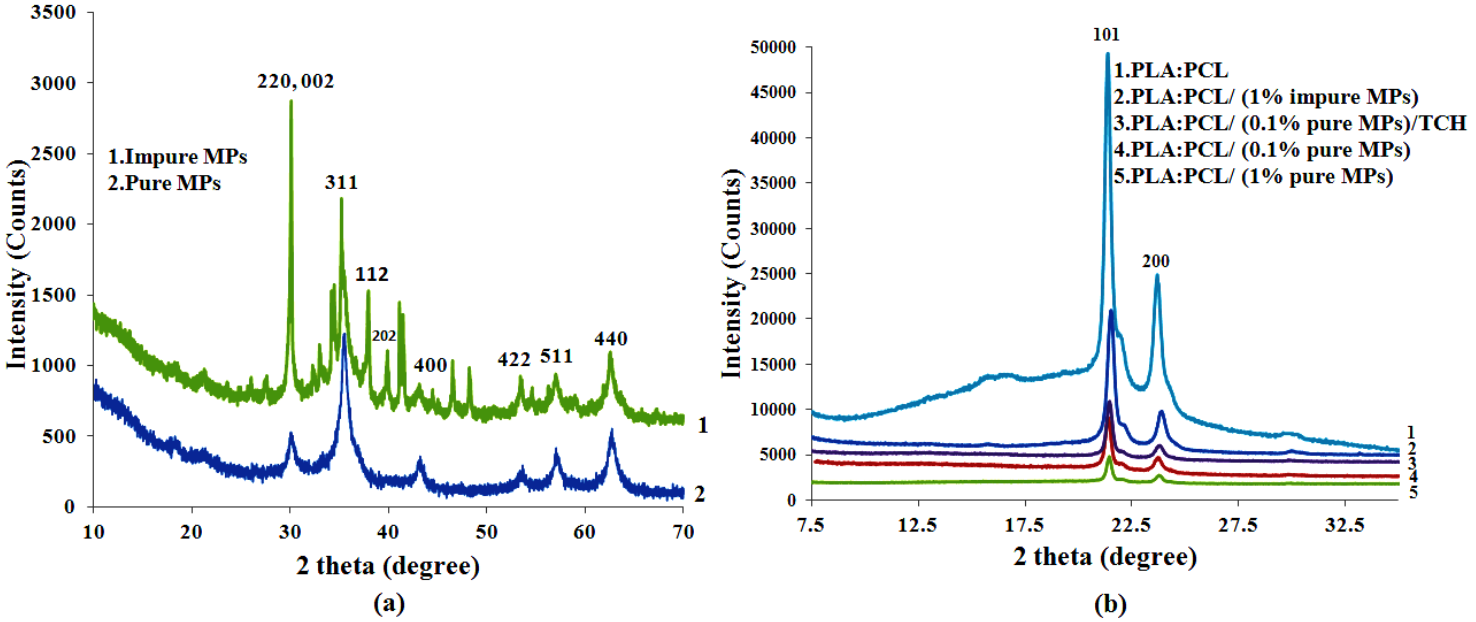
Intensity (Counts)
2 theta (degree)
(a)
1.Impure MPs
2.Pure MPs
220, 002
311
112
202
400
422
511
440
1
2
101
200
1.PLA:PCL
2.PLA:PCL/ (1% impure MPs)
3.PLA:PCL/ (0.1% pure MPs)/TCH
4.PLA:PCL/ (0.1% pure MPs)
5.PLA:PCL/ (1% pure MPs)
(b)

FIGURE 8

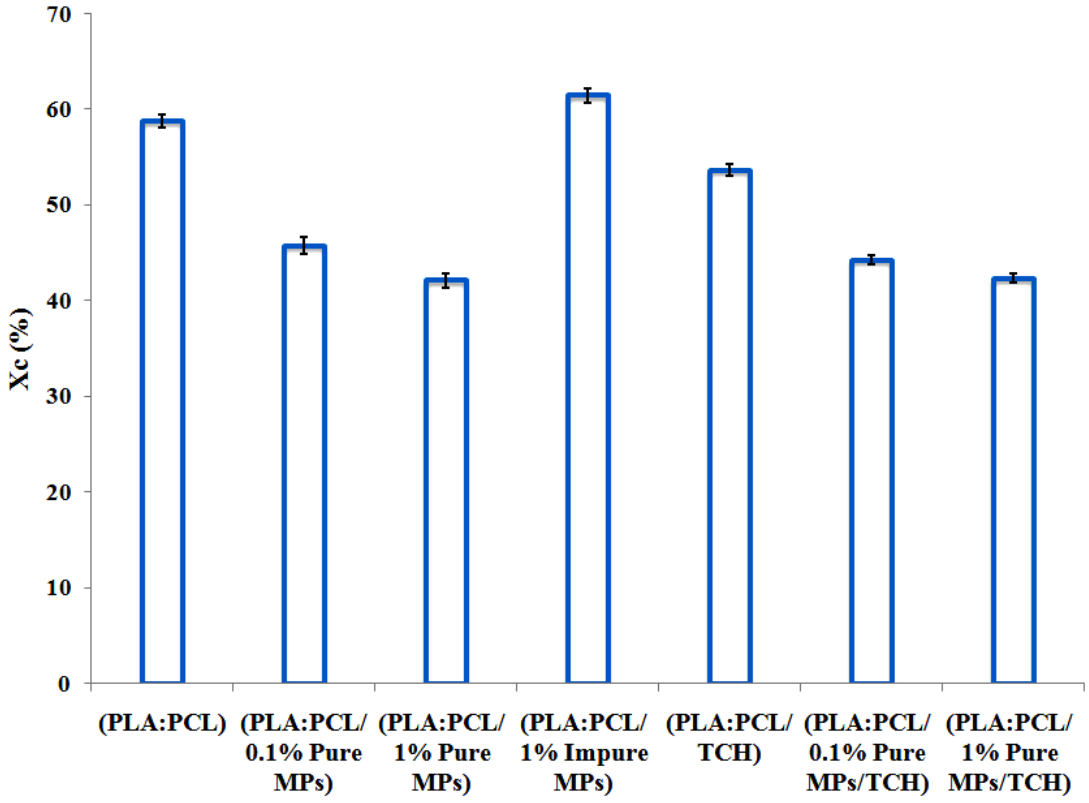
70
60
50
40
30
20
10
0
Xc (%)
(PLA:PCL)
(PLA:PCL/ 0.1% Pure MPs)
(PLA:PCL/ 1% Pure MPs)
(PLA:PCL/ 1% Impure MPs)
(PLA:PCL/ TCH)
(PLA:PCL/ 0.1% Pure MPs/TCH)
(PLA:PCL/ 1% Pure MPs/TCH)

FIGURE 9

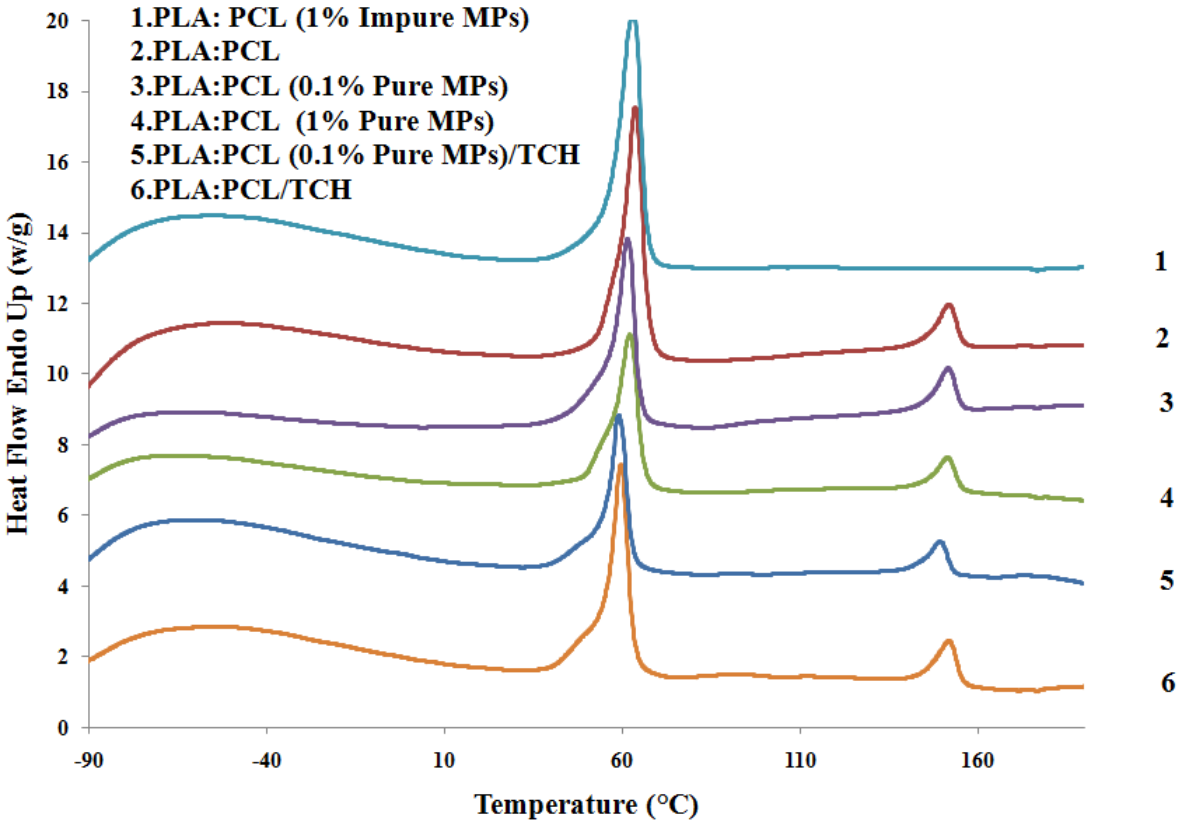
1.PLA: PCL (1% Impure MPs)
2.PLA:PCL
3.PLA:PCL (0.1% Pure MPs)
4.PLA:PCL (1% Pure MPs)
5.PLA:PCL (0.1% Pure MPs)/TCH
6.PLA:PCL/TCH
Heat Flow Endo Up (w/g)
Temperature (°C)
20
18
16
14
12
10
8
6
4
2
0
-90
-40
10
60
110
160
1
2
3
4
5
6

FIGURE 10

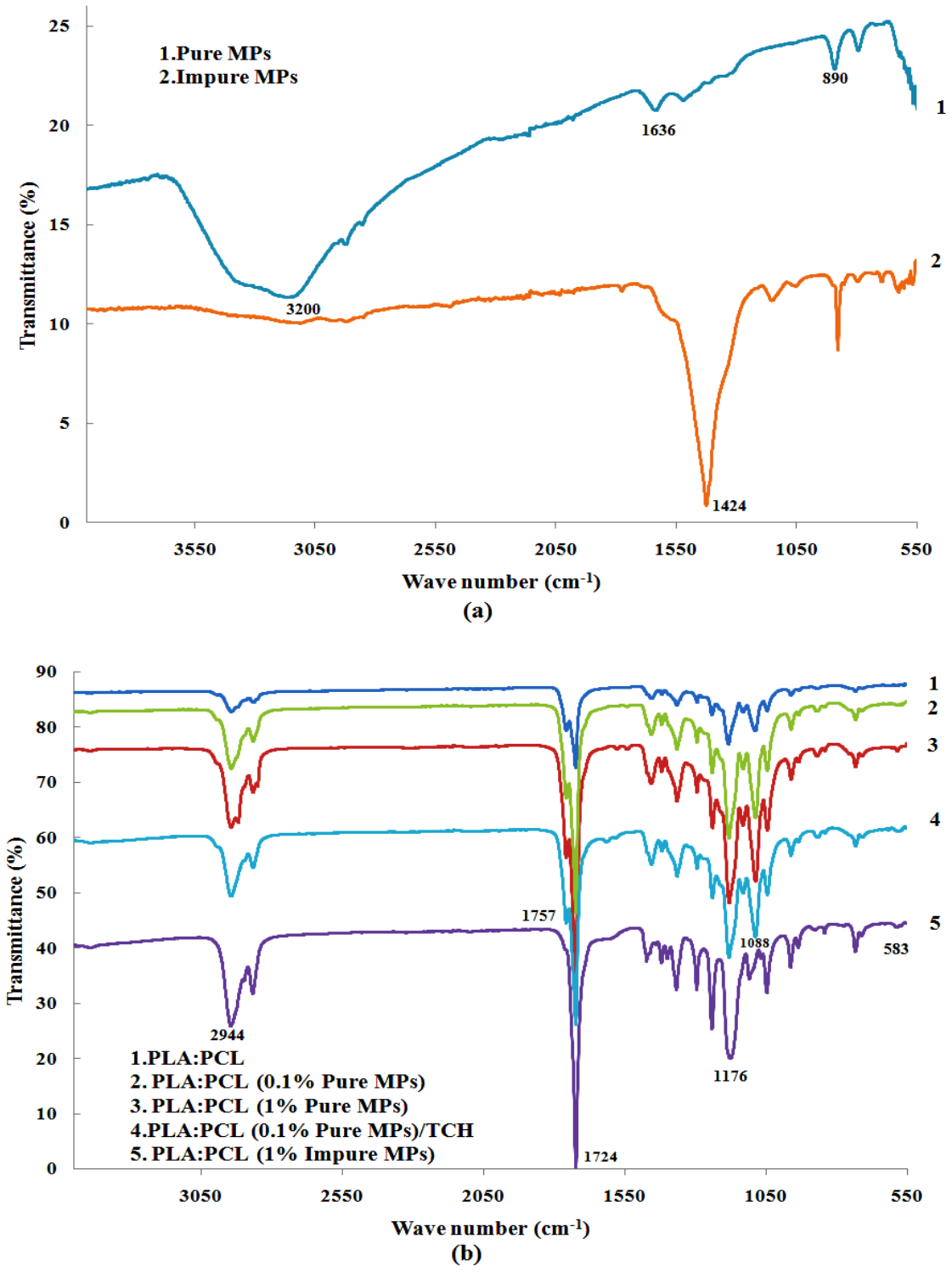
1.Pure MPs
2.Impure MPs
890
1636
3200
1424
1
2
Transmittance (%)
Wave number (cm-1)
(a)
1757
1088
583
2944
1176
1724
1.PLA:PCL
2. PLA:PCL (0.1% Pure MPs)
3. PLA:PCL (1% Pure MPs)
4.PLA:PCL (0.1% Pure MPs)/TCH
5. PLA:PCL (1% Impure MPs)
3
4
5
Transmittance (%)
Wave number (cm-1)
(b)

FIGURE 11

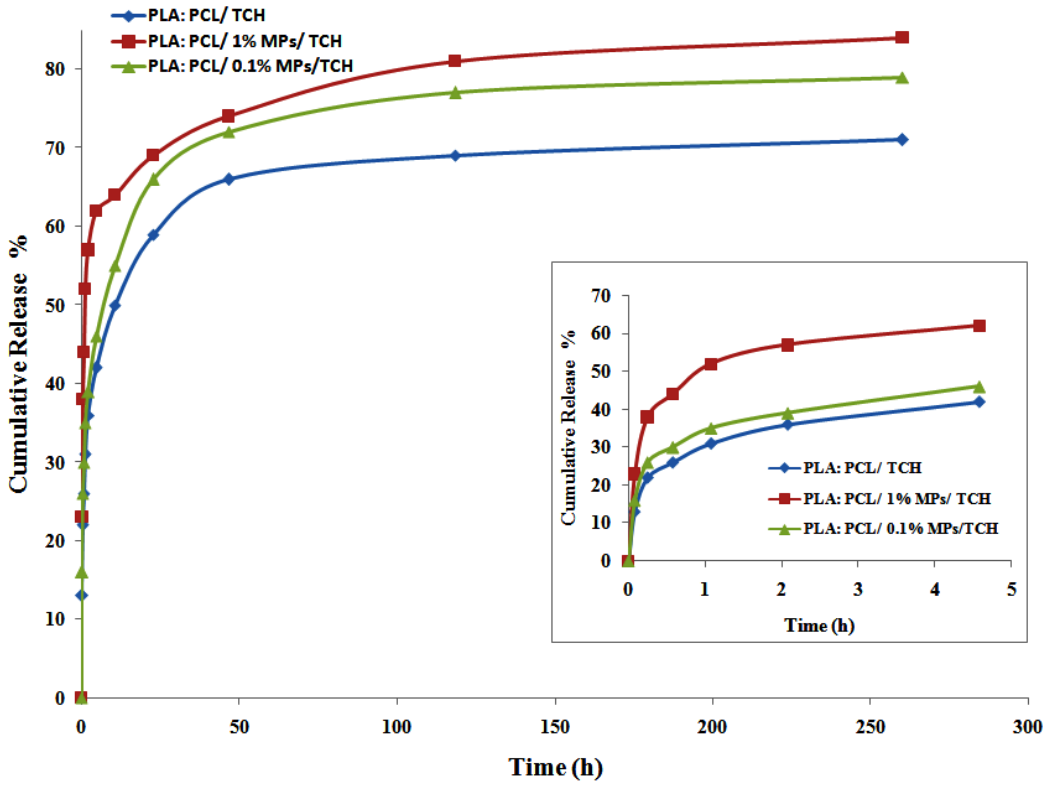
PLA: PCL/ TCH
PLA: PCL/ 1% MPs/ TCH
PLA: PCL/ 0.1% MPs/TCH
Cumulative Release %
Time (h)
0
10
20
30
40
50
60
70
80
0
50
100
150
200
250
300
Cumulative Release %
Time (h)
0
1
2
3
4
5
0
10
20
30
40
50
60
70
PLA: PCL/ TCH
PLA: PCL/ 1% MPs/ TCH
PLA: PCL/ 0.1% MPs/TCH

FIGURE 12

TABLE 1 Summary of average fiber diameters[a] (nm) for electrospun composite fibers with MPs and TCH.

	MP 0%	MP 0.01wt%/v	MP 0.1 wt%/v	MP 1 wt%/v	MP 0 wt%/v and TCH 5 wt%	MP 0.1 wt%/v and TCH 5 wt%	MP 1 wt%/v and TCH 5 wt%
Pure MPs	814 (±15)	711 (±15)	685 (±20)	583 (±25)	623 (±15)	562 (±20)	491(±20)
Impure MPs	814 (±15)	80 (±15)	62 (±15)	51 (±15)	–	–	–

[a]*The numbers in parenthesis are the standard deviations.*

TABLE 2 DSC results for PLA and PLA: PCL based composite fibers with pure and impure MPs and TCH[a].

Sample	T_g(°C) PCL	T_m(°C) PCL	T_c(°C) PLA	T_m (°C) PLA
PCL (fibers)	–58.0	63.1	–	–
PLA: PCL	–52.2	63.8	84.0	152.5
PLA: PCL (0.1% pure MPs)	–53.0	61.5	82.7	151.7
PLA: PCL (1% pure MPs)	–58.2	62.2	81.6	151.5
PLA: PCL (1% impure MPs)	–53.2	63.1	88.0	–
PLA: PCL / TCH	–58.5	59.6	105.8	152.0
PLA: PCL(0.1% pure MPs)/ TCH	–60.5	59.2	101.8	149.4

[a] Calculations were repeated for three sets of samples. The standard deviations for the T_g, T_c and T_m values were less than 0.5°C.

TABLE 3 Drug release parameters obtained by fitting drug release experimental data to five different mathematical models for drug release kinetics.

Mathematical model	Zero order	First order	Higuchi	Ritger-Peppas	Zeng
Equation	$M_t/M_\infty = K_0 t$	$M_t/M_\infty = 1 - e^{-K_1 t}$	$M_t/M_\infty = K_H t^{1/2}$	$M_t/M_\infty = K_R t^n$	**
PLA: PCL	K_0=0.002 R^2=0.434	K_1=0.582 R^2=0.839	K_H=0.038 R^2=0.691	K_R=1.262 n=0.204 R^2=0.927	K_{on}=0.0034 h^{-1} K_{off}=0.0033 h^{-1} K_s=1.160 h^{-1} *$\Delta G = -2.0\times10^{-22}$ J R^2= 0.920
PLA:PCL/0.1 % pure MPs	K_0=0.0022 R^2=0.451	K_1=0.625 R^2=0.808	K_H=0.042 R^2=0.705	K_R=1.127 n=0.193 R^2=0.950	K_{on}=0.0069 h^{-1} K_{off}=0.0065 h^{-1} K_s=1.864 h^{-1} *$\Delta G = -2.6\times10^{-22}$ J R^2=0.923
PLA:PCL/1% pure MPs	K_0=0.0019 R^2=0.348	K_1=2.097 R^2=0.856	K_H=0.037 R^2=0.560	K_R=0.806 n=0.138 R^2=0.938	K_{on}=0.0041 h^{-1} K_{off}=0.0059 h^{-1} K_s=3.764 h^{-1} *$\Delta G = 1.47\times10^{-21}$ J R^2=0.956

**$M_t/M_\infty = [K_{off}/(K_{on} + K_{off})](1 - e^{-K_s t}) + [K_{on}/(K_{on} + K_{off})](1 - e^{-K_{off} t})$

*$\Delta G = -k_B T \ln(K_{on}/K_{off})$, where k_B is the Boltzmann's constant and T is the absolute temperature (300 K).